Materials Research Bulletin 48 (2013) 3211–3217

Contents lists available at SciVerse ScienceDirect

Materials Research Bulletin

journal homepage: www.elsevier.com/locate/matresbu

Effect of calcination temperature on structural and photocatalyst properties of nanofibers prepared from low-cost natural ilmenite mineral by simple hydrothermal method

Athapon Simpraditpan [a], Thanakorn Wirunmongkol [b], Sorapong Pavasupree [b,*], Wisanu Pecharapa [a,c]

[a] College of Nanotechnology, King Mongkut's Institute of Technology Ladkrabang, Ladkrabang, Bangkok 10520, Thailand
[b] Department of Materials and Metallurgical Engineering, Faculty of Engineering, Rajamangala University of Technology Thanyaburi, Klong 6, Pathumthani 12110, Thailand
[c] Thailand and Center of Excellence in Physics (ThEP Center), Commission on Higher Education, 328 Si Ayutthaya Rd., Bangkok 10400, Thailand

ARTICLE INFO

Article history:
Received 16 July 2012
Received in revised form 24 March 2013
Accepted 29 April 2013
Available online 27 May 2013

Keywords:
A. Composites
A. Nanostructures
B. Chemical synthesis
D. Catalytic properties

ABSTRACT

Titanate nanofibers were synthesized via the hydrothermal method (120 °C for 72 h) using natural ilmenite mineral ($FeTiO_3$) as the starting material. The samples were characterized by X-ray diffraction (XRD), X-ray fluorescent (XRF), scanning electron microscopy (SEM), transmission electron microscopy (TEM), and Brunauer–Emmett–Teller (BET) for specific surface area. The nanofibers were 20–90 nm in diameter and 2–7 μm in length. The as-synthesized nanofibers calcined at 300–400 °C showed TiO_2 (B) whereas the nanofibers calcined at 500 °C revealed a mixture of two phases of TiO_2 (B) and anatase. The nanofibers calcined at high temperature of 600–1000 °C showed a mixture of tri-crystalline of anatase, rutile, and Fe_2O_3. The rutile phase increased with increasing calcination temperature. The nanofibers calcined at 300–700 °C maintained their structure while the morphology of the nanofibers calcined at 800–1000 °C transformed into submicron rod-like structure. This increase of calcination temperature led to the phase transformation from thermodynamically metastable anatase to the most stable form of rutile phase. The crystallite size of prepared samples increased with increasing calcination temperature. Interestingly, with increasing calcination temperature, the absorption edge of the prepared samples shows an obvious shift to visible light region due to the change of crystallite phase and increased crystallite size. Therefore, the band gap energy of the prepared samples became narrower with increasing calcination temperature. Furthermore, the photocatalytic activity of the nanofibers calcined at 400 °C for 2 h was found to be not merely higher than those of the commercially available TiO_2 nanoparticles powders (P-25, JRC-01, and JRC-03) but also the highest of all the samples in this study.

1. Introduction

Over the past three decades, nanostructured materials derived from TiO_2 have been regarded as the most suitable semiconductor in such applications as photocatalyst of water splitting [1–5] and degradation of organic contaminants in water treatment [6–13]. The rate of the photocatalytic reaction is controllable at various steps in the process: light absorption, transport of photogenerated charges (electron (e^-) and hole (h^+)) onto the photocatalyst surface, and recombination of e^- and h^+ on the photocatalyst surface [14]. Therefore, the crystalline structure and surface morphology of a photocatalyst, such as the particle shape and size, are significant parameters in photocatalytic reactions [15–17]. In addition, TiO_2 derived materials possess a number of good points, such as high photovoltaic effect, medium dielectric permittivity, high chemical stability, and low toxicity [18]. Thus, TiO_2 derived materials were introduced into a number of applications, e.g., catalysts [19], gas sensors [20], and dye-sensitized solar cells [21,22].

TiO_2 exists in various crystalline structures, i.e., anatase (band gap energy 3.2 eV), rutile (band gap energy 3.0 eV), brookite, and monoclinic of TiO_2 (B) [18,23]. Several methods were employed in the preparation of the TiO_2-derived nanomaterials, examples of which were inert gas condensation [24] sol–gel method [25,26] electrospinning [27,28], and hydrothermal [29–38]. In our previous works, the hydrothermal method was selected to synthesize nanofibers from leucoxene mineral because it was simple, low-cost, and environmentally friendly [38,39].

The nanofibers in this study were prepared by the simple hydrothermal method using inexpensive natural ilmenite mineral (~0.5–0.7 dollar/kg) as the starting material. The calcined nanofibers were treated with the calcination process. The chemical composition, crystalline structures, morphology, and BET specific

* Corresponding author. Tel.: +66 2 549 3480; fax: +66 2 549 3483.
E-mail addresses: sorapongp@yahoo.com, sorapong.p@en.rmutt.ac.th (S. Pavasupree).

0025-5408/$ – see front matter © 2013 Elsevier Ltd. All rights reserved.
http://dx.doi.org/10.1016/j.materresbull.2013.04.083

surface areas of the prepared samples and calcined nanofibers were investigated and reported. Besides, the effects of calcination temperature on structural and photocatalyst properties of the nanofibers prepared from natural ilmenite mineral by the hydrothermal method were discussed.

2. Experimental procedure

2.1. Preparation of nanofibers

The nanofibers were prepared by the hydrothermal method in which natural ilmenite mineral (Sakorn Minerals Co., Ltd., Thailand) was used as the starting material. 5 g of ilmenite mineral and 10 M NaOH aqueous solution (200 ml) were placed inside a Teflon-lined stainless autoclave. The autoclave was heated and stirred at 120 °C for 72 h. Afterward, the mixture was cooled down to room temperature and was washed with 0.1 M HCl aqueous solution and DI water a number of times. Then, the precipitated sample was dried at 100 °C for 12 h.

2.2. Characterization

The chemical composition of the ilmenite mineral and that of the as-synthesized sample were evaluated by X-ray fluorescence (XRF, Philips, PW-2404, 4 kW). The microstructures of the ilmenite mineral, the as-synthesized nanofibers and the calcined nanofibers were investigated by scanning electron microscopy (SEM; JEOL, JEM-6510) and transmission electron microscopy (TEM; JEOL, JEM-2010). The X-ray diffraction (XRD) patterns of the as-synthesized samples were obtained with PANalytical diffractometer (X'Pert PRO MPD model pw 3040/60) using Cu Kα ($\lambda = 0.154$ nm) irradiation at a scan rate (2θ) of 0.02° s^{-1} and a 2θ range of 5–80° operated at 40 kV and 30 mA. The BET specific surface areas of the samples were measured using nitrogen adsorption (Quantachrome Instruments, Autosorb-1).

2.3. Photocatalytic activity measurement

The photocatalytic activity was measured through the formation rate of I_3^- due to the oxidation photoreaction of I^- to I_2 in excess I^- conditions [15]. A reaction system was set up by adding 50 mg of a sample powder into 10 ml of 0.2 M of potassium iodide (KI) aqueous solution; the mixture was then stirred and irradiated at room temperature with UV light with maximum emission of approximately 365 nm. Following the irradiation for 15, 30, 45, and 60 min, the suspension was withdrawn and centrifuged. After the clear supernatant was diluted 10 times, the concentration of liberated I_3^- ions was determined by the absorbance at 288 nm using an UV-Vis spectrophotometer (Shimadzu UV 2450). The molar extinction coefficient was found to be 4.0×10^4 $(cm\ mol/l)^{-1}$; no I_3^- formation was observed when the experiments were performed in the dark or in the absence of the TiO_2 samples. Three different commercially available TiO_2 nanoparticle powders, i.e., P-25 (Nippon Aerosil Co., Ltd., Japan), JRC-01, and JRC-03 (The Catalysis Society of Japan) were tested for use as reference.

3. Results and discussion

3.1. As-synthesized nanofibers

After the reaction in the hydrothermal process, the as-synthesized nanopowders become brown (Fig. 2(b)) while the starting ilmenite mineral is black (Fig. 2(a)). The findings indicated that a large fraction of Fe impurities could be eliminated by the NaOH (aq.) hydrothermal treatment and neutralization/washing processes [34]. The chemical composition of ilmenite mineral and that of the as-synthesized sample were evaluated by XRF. Following the hydrothermal process, the percentage of impurities (Fe_2O_3, Al_2O_3, SiO_2, MnO) decreased while that of TiO_2 increased from 66.99 to 76.21 wt%. The results were consistent with those of leucoxene mineral and nanofibers from leucoxene mineral in our previous works [38,39], but the as-synthesized nanofibers showed a higher percentage of Fe_2O_3 than the nanofibers prepared from leucoxene mineral. The aforementioned could be due to solubility of the impurities in NaOH and HCl aqueous solutions during preparation process [14,15]. Recent studies indicated Fe doping significantly enhanced the optical response of visible light owing to the reduced band gap energy [16], probably contributing to the brown color of the as-synthesized sample in this research. The nanofibers doped with Fe could be an alternative material with high potential for use as photocatalyst in hydrogen generation, dye-sensitized solar cell (DSSC), and decomposition of organic dyes.

Fig. 1(a) shows the XRD patterns of the prepared samples compared with the starting ilmenite mineral. The XRD pattern of the starting ilmenite mineral emerged in rutile phase, while the structure of the as-synthesized nanofibers revealed the hydrogen

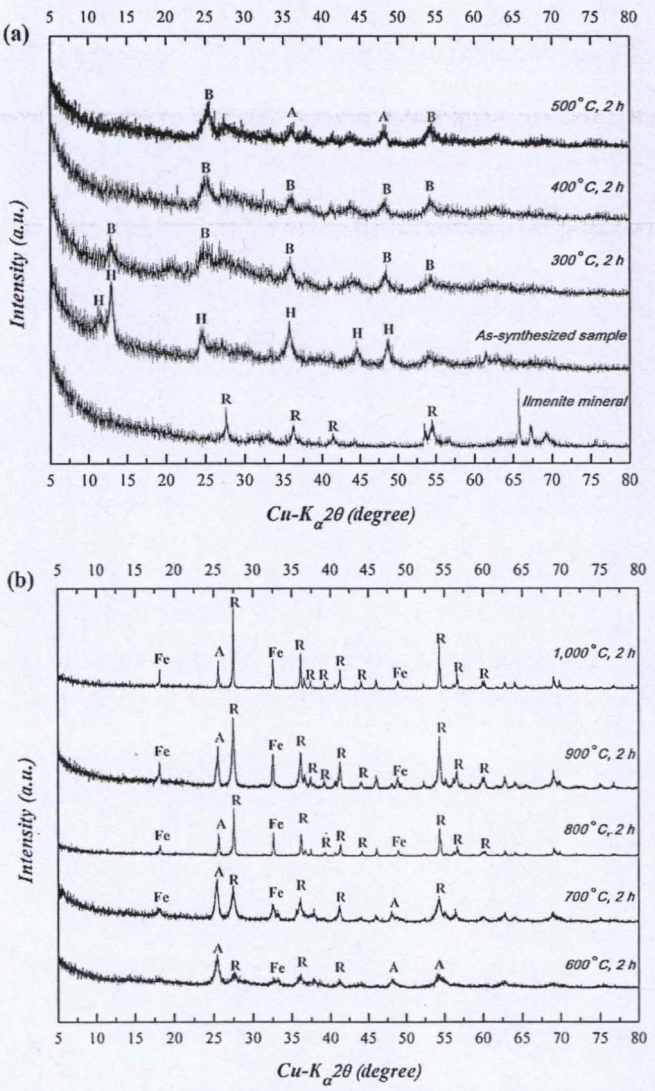

Fig. 1. XRD patterns of the starting natural ilmenite mineral, the as-synthesized nanofibers, and the calcined nanofibers for 2 h at (a) 100–500 °C and (b) 600–1000 °C; A: anatase TiO_2, B: TiO_2 (B), H: hydrogen titanate, and R: rutile TiO_2.

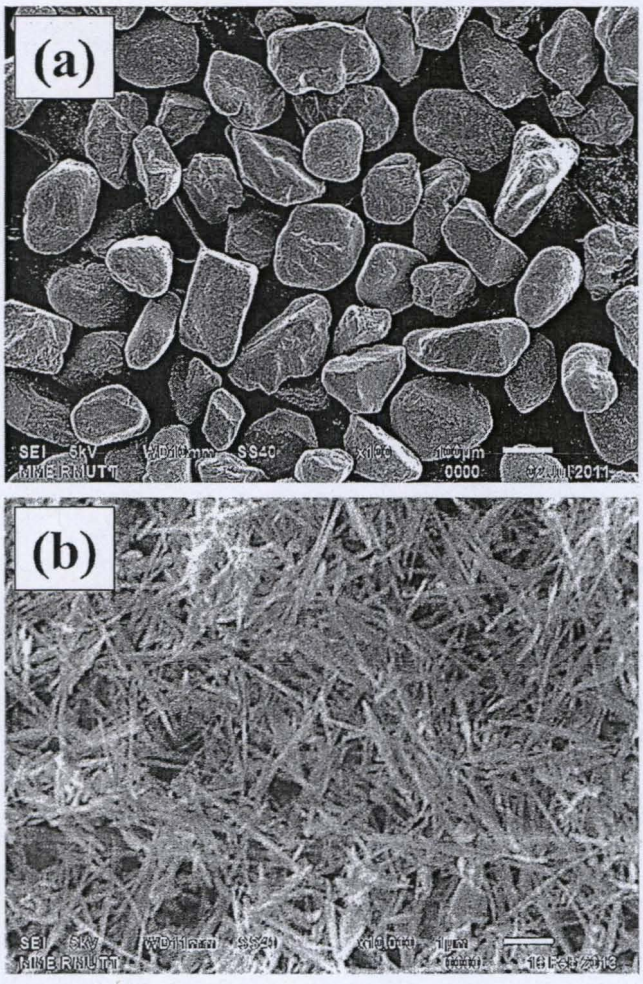

Fig. 2. SEM images of (a) the starting ilmenite mineral and (b) the as-synthesized nanofibers.

titanate $H_2Ti_xO_{2x+1}$, e.g., trititanate ($H_2Ti_3O_7$) [18,31]. The results were similar to those of leucoxene mineral and nanofibers from leucoxene mineral in our previous works [38,39]. The difference points between nanofibers using ilmenite mineral as the starting materials for this study and nanofibers using leucoxene mineral as the starting materials for previous work [38] were discussed. Interestingly, the chemical composition of nanofibers using leucoxene mineral as the starting materials consist of Fe_2O_3 similar to this study. However, nanofibers using leucoxene mineral as the starting materials showed less the percentage of Fe_2O_3 than nanofibers using ilmenite mineral as the starting materials that is 2.26% and 21.80%, respectively [38,40]. This difference may be result in the photocatalytic activity [41,42].

The diffraction peaks of other impurities, such as NaCl and rutile phase of the starting natural ilmenite mineral, were not observed. This was due to the fact that Na content in the nanofibers could be minimized by repeated ion-exchanging treatment with HCl leaching and water washing [34,36,43]. Nevertheless, compared with the titanate nanotubes, the nanofibers tended to contain more residual Na ions under the same ion-exchanging conditions due to the geometry of the nanofibers, i.e., more solid and thicker structure, and alkali-metal hexatitanates ($A_2Ti_6O_{13}$, A = Na, K, Rb) tended to be in the form of stable solid fibrous structure and was not easily removed with the aqueous HCl treatment at room temperature [34].

Fig. 2 shows the SEM images of the starting ilmenite mineral and as-synthesized sample. The starting ilmenite mineral is in granule form of 150–200 μm in diameter (Fig. 2(a)). The as-synthesized nanofibers possess the fiber-like morphology with the lengths and diameters of 2–7 μm and 20–90 nm, respectively (Fig. 2(b)). Furthermore, most of the nanofibers tend to stick together in bundles, thus causing some of the nanofibers to appear thicker than others. TEM experiment was conducted to prove that nanofibers were solid (not hollow). The TEM image of the as-synthesized nanofibers was illustrated in Fig. 3, which showed the as-synthesized sample to be solid (not hollow), indicating the structure of nanofiber.

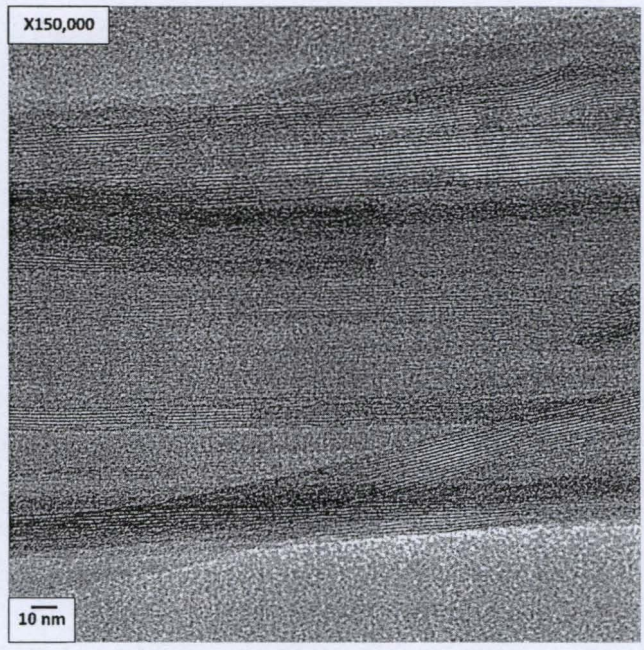

Fig. 3. TEM image of the as-synthesized nanofibers at 150,000× magnification.

Interestingly, the BET specific surface area of the as-synthesized nanofibers was about 50 m^2/g, while the BET specific surface area of the starting natural rutile sand was about 0 m^2/g. Increased surface areas are generally accomplished by the synthesis of small particles with high surface to volume ratios or by the manufacture of nanostructured materials from bulk substrates.

3.2. Nanofibers with calcination treatment (300–500 °C)

Fig. 1(a) also shows the XRD patterns of the prepared samples calcined for 2 h at 300, 400, and 500 °C. After calcination at the temperature range of 300–400 °C, the calcined samples demonstrated TiO_2 (B). The nanofibers were dehydrated and re-crystallized into the metastable form of TiO_2 (B) [5,33–38]. Moreover, the peak intensity corresponding to the TiO_2 (B) decreased as the calcination temperature increased. At 500 °C, the calcined nanofibers revealed a bi-crystalline mixture consisting of TiO_2 (B) and anatase TiO_2. Recent research studies found a bi-crystalline mixture consisting of TiO_2 (B) and anatase TiO_2 nanostructured not merely showed similar formation in the temperature ranges of 100–500 °C [37], 300–600 °C [44] or 400–600 °C [45] but promoted great H_2 evolution from neat ethanol as well [5,38,46].

Fig. 4 shows the SEM images of the as-obtained nanofibers calcined for 2 h at 300, 400, and 500 °C. From the SEM images, the nanofibers calcined for 2 h at 300–500 °C maintained their nanofiber morphology [31]. In many research studies, the nanotube structure was frequently investigated due to its high surface area; however, titanate nanotubes with free-alkali ions

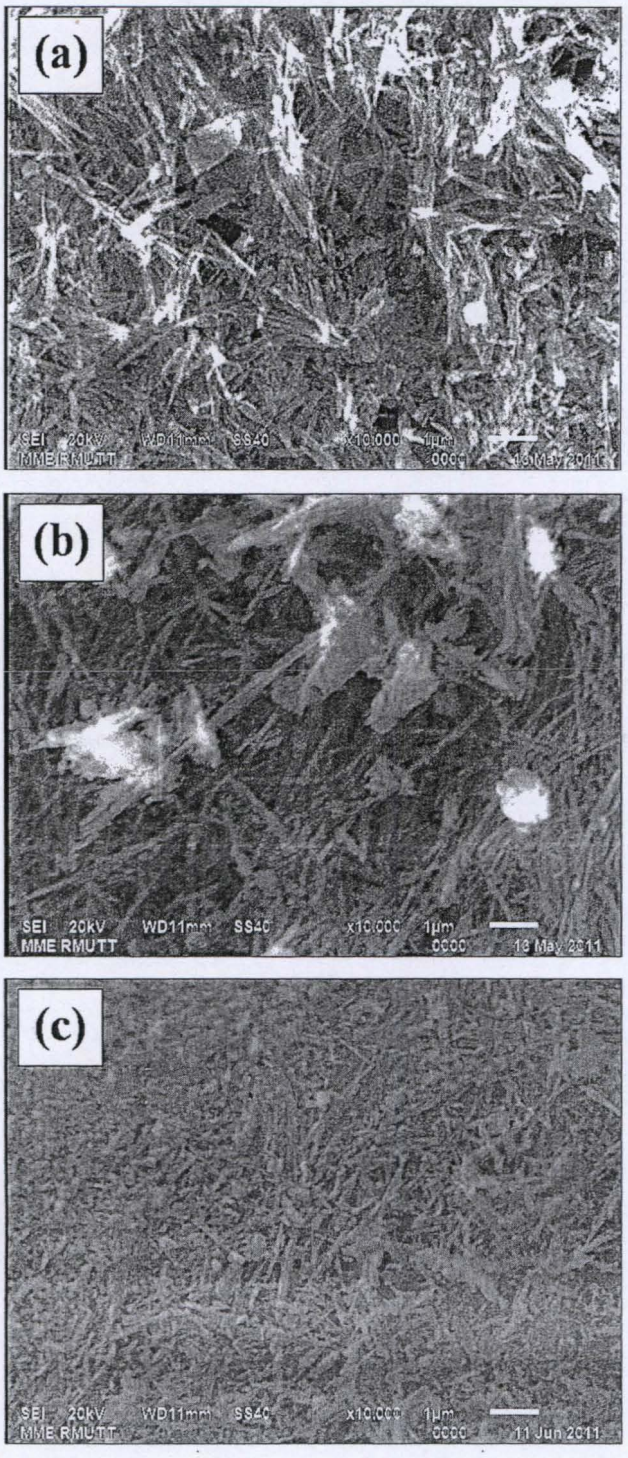

Fig. 4. SEM images of the calcined nanofibers for 2 h at (a) 300 °C, (b) 400 °C, and (c) 500 °C.

were typically unstable at high temperatures (at ~500 °C) and converted into anatase particles [33–35,37]. To maintain the 1-D nanostructure at higher temperatures (typically at 500–800 °C), solid nanowires or nanofibers are more preferable.

3.3. Nanofibers with calcination treatment (600–1000 °C)

The XRD patterns of the prepared samples calcined at 600, 700, 800, 900, and 1000 °C for 2 h are shown in Fig. 1(b). The prepared samples consisted of a mixture of anatase, rutile phase of TiO_2 [4,5], and Fe_2O_3. At 600–700 °C, the crystalline of anatase phase of TiO_2 became unstable, TiO_2 (B) disappeared, and the transformation from anatase phase TiO_2 to rutile phase TiO_2 began at this temperature range [30,47]. Consequently, the calcination temperature rose, increase in rutile phase TiO_2 was observed, especially at the 800–1000 °C, at which the rutile phase TiO_2 was dominant while the anatase phase TiO_2 was almost non-existent. Furthermore, recent papers reported that doping Fe into TiO_2 enabled the photon absorbing zone of TiO_2 to extend from UV toward visible light as well as reduced TiO_2 band gap energy from 3.2 to 2.67 eV [48,49].

Table 1
Effect of temperature on physicochemical properties of the prepared samples.

Materials	Calcination temperature (°C)	Anatase (1 0 1) over rutile (1 1 0) ratio (A:R)	Crystalline size (nm)[a]	
			Anatase (1 0 1)	Rutile (1 1 0)
Nanofibers from ilmenite	As-synthesized	–	–	–
	300	–	–	–
	400	–	–	–
	500	–	–	–
	600	73:37	21	12
	700	49:51	29	19
	800	28:72	33	41
	900	32:68	49	142
	1000	22:78	142	142

[a] Calculated by using Sherrer formula.

The phase content between anatase and rutile was estimate from the equation: $FR = 1/\{1 + 0.79[IA(1\,0\,1)/IR(1\,1\,0)]\}$ suggested by Spurr and Myers [50]. The effects of calcination temperatures on phase content and crystalline size of prepared samples are shown in Table 1. This observation shows that with increasing calcination temperature from 600 to 1000 °C, the trend of anatase ratio gradually decreased, meanwhile the rutile ratio became stronger. This result indicates that the increase of calcination temperature led to the phase transformation from thermodynamically metastable anatase to the most stable form of rutile phase [51–53]. This phenomenon relates to an enhancement of crystallization of rutile phase. Typically, phase transformation is supplemented with crystal growth [51].

From the XRD spectra, the crystallite sizes can be calculated by the Debye–Scherrer formula $D = K\lambda/\beta\cos\theta$, where D is the crystallite diameter in nm, K is the shape constant (0.90), λ is the wavelength of X-ray (1.541874 Å), β is the peak width (in rad) at half-maximum height and h is the Bragg angle. As the calcination temperature is raised, XRD reflections corresponding to both the anatase and rutile phase become narrower, which indicates the increase of crystallite size [51,53]. The crystallite size was shown in Table 1. The crystallite size of samples calcined at lower temperature (below 800 °C) increased slightly from about 21 to 33 nm for anatase phase and 12 to 41 nm for rutile phase. At higher temperature (1000 °C) caused rapid increase of crystallite size up to about 142 nm for both the anatase and rutile. This result is similar to study by Górska et al. [54].

Fig. 5 depicts the SEM images of the prepared samples calcined at 600, 700, 800, 900, and 1000 °C for 2 h. The nanofibers calcined at 600–700 °C for 2 h maintained their nanofiber morphology (Fig. 5(a) and (b)). Typically, the TiO_2-derived nanotubes after heat-treatment at 400 °C (anatase phase) were destroyed and transformed into nanoparticles [33,55]. However, in this work, the prepared samples calcined at high temperatures of 600–700 °C for 2 h were stable. Therefore, the prepared samples can be utilized in various applications operated at high

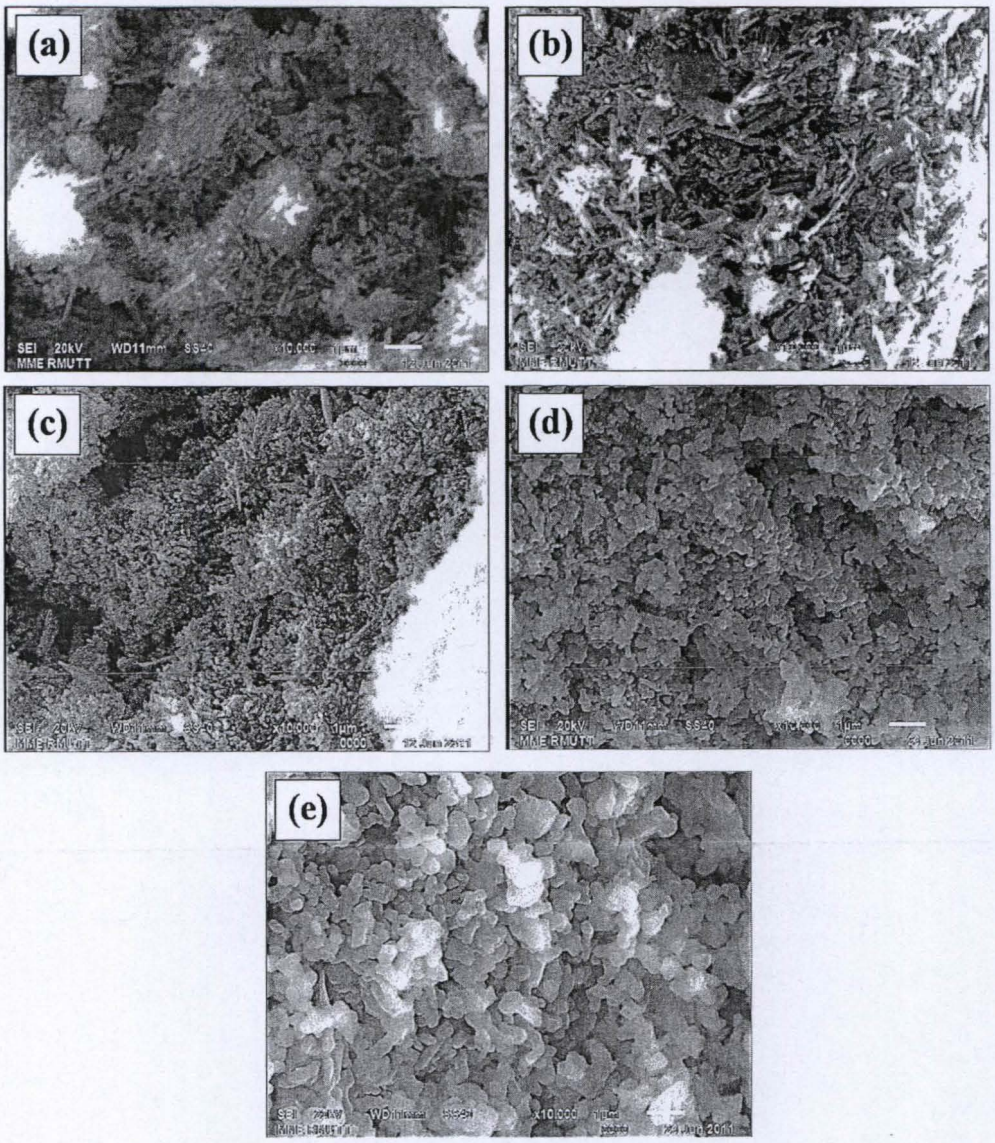

Fig. 5. SEM images of the calcined nanofibers for 2 h at (a) 600 °C, (b) 700 °C, (c) 800 °C, (d) 900 °C, and (e) 1000 °C.

temperatures. In addition, the prepared samples calcined at 800–1000 °C for 2 h showed submicron particle structure of rutile TiO_2 (Fig. 5(c)–(e)) Recent papers reported that the submicron particle structure of rutile TiO_2, caused by increasing calcination temperature, decreased the BET specific surface area of the nanofibers [5,33,35,38].

Other studies reported the influence of phase composition and BET specific surface area of TiO_2 nanostructured on the photocatalyst properties. Indeed, it was found that the photocatalyst properties of anatase phase of TiO_2 were better than those of rutile [4,5,38]. However, the band gap of rutile (3.0 eV) was lower than that of anatase (3.2 eV); as such, rutile should be more easily photo-excited. The high recombination possibility of photo-generated electrons and holes was the major limiting factor for the indigent photocatalytic activity of rutile [5,38]. Generally, phase composition, specific surface area, pore size distribution, particle morphology, particle aggregation, and impurities can play a crucial role in determining the efficiency of specific applications [56]. Thus, the calcination process is required to control the crystalline structure of TiO_2 nanofibers.

3.4. UV–Vis diffuse reflectance spectrum

The UV–Vis absorption spectra of the samples were recorded using a UV–Vis spectroscopy (UV-2401, Shimadzu). The band gap energy (E_g) was estimated from absorption edge from equation as shown in Eq. (1) by Oregan and Grätzel [57].

$$E_g = \frac{hC}{\lambda} \quad (1)$$

where h is the Planks constant = 6.623×10^{-34} J s, C the speed of light = 3.0×10^8 m/s and λ is the cut off wavelength (m).

The influence of temperature on the light absorption characteristic of prepared samples investigated from the as-synthesized and nanofibers calcined at 400, 700, and 1000 °C for 2 h and shown in Fig. 6. A significant increase at wavelengths shorter than 400 nm could be explained to absorption of light caused by the excitation of electrons from the valence band to the conduction band of TiO_2 [51,58]. A shift to visible light region of the absorption of the prepared samples was observed for the as-synthesized and nanofibers calcined at 400, 700, and 1000 °C for 2 h. The differences

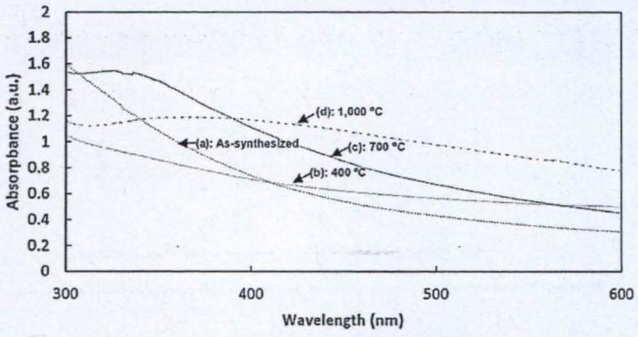

Fig. 6. UV–Vis spectra of the as-synthesized nanofibers and the calcined nanofibers for 2 h at various temperatures.

in absorption were described to the change of crystallite size and phase structure [51,53]. The absorption edges shifted toward longer wavelengths were attributed to the existence of iron (Fe) in the prepared samples, the excitation of 3d electron of Fe^{3+} ion to the TiO_2 conduction band (charge transfer transition) may be extended of absorption of the prepared samples from UV toward visible light [41,58,59]. This correlates with the appearance of the brown coloration of the prepared samples.

The band gap energy of the as-synthesized and nanofibers calcined at 400, 700, and 1000 °C for 2 h estimated from Eq. (1) was about 3.80, 2.62, 2.32, and 2.12 eV, respectively. Recently paper, reported the Fe_2O_3/TiO_2 composite showed narrower band gap energy was about 2.20–2.63 eV [42]. The difference in band gap energy is due to the result of the change of crystallite size and phase composition in the prepared samples [51,54]. This data showed that the band gap of prepared samples became narrower with increasing calcination temperature. This result due to following factor, the first reason, an increase in crystallite size leading to the decrease of band gap energy, which was in correspond with recently work reported by Xiao et al. [60] and the second, after calcination at 400, 700, and 1000 °C for 2 h, lower value of band gap energy for samples was observed, due to phase transformation from anatase to rutile [51,53,54]. However, the band gap energy of the as-synthesized showed larger gap may be cause by titanate structure of this sample [61].

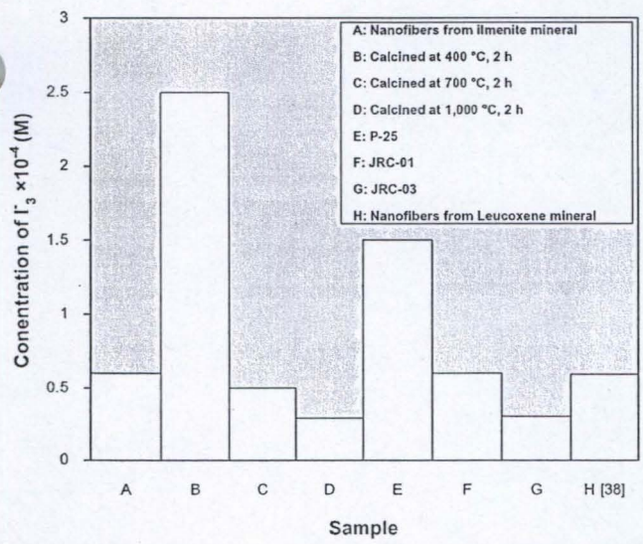

Fig. 7. Photocatalytic activity (I_3^- concentration) of the as-synthesized nanofibers, the calcined nanofibers for 2 h at various temperatures, commercial TiO_2 nanoparticles (P-25, JRC-01, and JRC-03), and nanofibers from leucoxene mineral.

3.5. Photocatalytic activity

Fig. 7 shows the photocatalytic activity of the as-synthesized nanofibers, nanofibers calcined at various temperatures for 2 h, and commercial grade TiO_2 nanoparticles, i.e., P-25, JRC-01, and JRC-03. The photocatalytic activities of all the samples calculated as the concentration of I_3^- in 10 ml of 0.2 M KI solution per unit mass. After UV irradiation for 60 min, the nanofibers calcined at 400 °C for 2 h showed the highest photocatalytic activity in which I_3^- concentration was approximately 2.50×10^{-4} M, whereas the nanofibers calcined at 1000 °C for 2 h showed the lowest photocatalytic activity with I_3^- concentration of roughly 0.29×10^{-4} M. The nanofibers calcined at 400 °C for 2 h exhibited higher photocatalytic activity (2.50×10^{-4} M) than the as-synthesized nanofibers, the nanofibers calcined at 700 °C, the as-synthesized nanofibers from leucoxene mineral, and commercial grade TiO_2 nanoparticles, i.e., P-25, JRC-01, and JRC-03, each of which respectively yielded I_3^- concentration of 0.60×10^{-4}, 0.50×10^{-4}, 0.59×10^{-4}, 1.50×10^{-4}, 0.60×10^{-4}, and 0.30×10^{-4} M. The results indicated that the calcination process significantly influenced the photocatalytic activity of the TiO_2 nanofibers, which could be attributed to: (1) the nanofibers calcined at 400 °C for 2 h showed TiO_2 (B), which promoted the photocatalytic activity [38]. The BET specific surface areas of the nanofibers calcined at low temperatures tended to be larger than those of the nanofibers calcined at high temperatures, and the larger BET specific surface area improved the photocatalytic activity [36,38,62–70]; (2) the hydrogen titanate structure of the as-synthesized nanofibers from ilmenite and leucoxene (previous work) [38] mineral had a larger band gap of approximately 3.80 eV corresponding to recently work, resulting in decreases in both photoreaction and photocatalytic activity of the as-synthesized sample [61,71–73]; (3) the nanofibers calcined at 700 and 1000 °C for 2 h showed not just a mixture of tri-crystalline phase of anatase, rutile, and Fe_2O_3 but also submicron particle structure. Generally, the rutile phase has high recombination rates of photogenerated e^- and h^+, leading to a decrease of photocatalytic activity [4,36,38,65]. Recent research studies reported that the submicron particle morphology decreased the specific surface areas and thereby the photocatalytic activity [36,38,62–68]. Thus, the photocatalytic activity decreased as the calcination temperature increased. In addition, although, nanofibers calcined at 700 and 1000 °C for 2 h showed the absorption higher than the nanofibers calcined at 400 °C for 2 h, but the narrower band gap energy is a result of the recombination of electron and hole that may be result in the decrease of the photocatatytic activity [74]. Furthermore, nanofibers calcined at 400 °C for 2 h showed greater photocatalytic activity than nanofibers calcined at 700 and 1000 °C for 2 h due to the overall increase in light absorbance [41].

4. Conclusion

The as-synthesized nanofibers (typically 2–7 μm in length and 20–90 nm in diameter) were prepared by simple hydrothermal processing using natural ilmenite mineral (rutile phase) as the starting material. The as-synthesized nanofibers were light brown-colored powder. The nanofibers calcined at 300–400 °C showed TiO_2 (B) whereas the nanofibers calcined at 500 °C revealed a mixture of TiO_2 (B) and anatase. The nanofibers calcined at high temperatures of 600–1000 °C showed a mixture of tri-crystalline of anatase, rutile, and Fe_2O_3. The rutile phase rose with increasing calcination temperature. Moreover, the nanofibers calcined at 300–700 °C maintained nanofiber structure while the morphology of nanofibers calcined at 800–1000 °C transformed into nanoparticles and submicron particles.

The transformation of anatase to rutile phase and the increase of crystallite size of prepared samples were observed with increasing calcination temperature. The absorption spectra of the as-synthesized and nanofibers calcined at 400, 700, and 1000 °C for 2 h shift to visible light region. The band gap energy of the as-synthesized and nanofibers calcined at 400, 700, and 1000 °C for 2 h was about 3.80, 2.62, 2.32, and 2.12 eV, respectively, indicating that the reduce of band gap energy of prepared samples was achieved with increasing calcination temperature. The photocatalytic activity of the nanofibers calcined at 400 °C for 2 h was not just higher than those of the commercial TiO_2 nanoparticles (P-25, JRC-01, and JRC-03) and nanofibers from leucoxene (previous work) but also the highest of all the samples. Therefore, the Fe-doped nanofibers have been increasingly applied to various applications, examples of which are in exciting low-energy visible wavelengths, photocatalyst of hydrogen generation, dye-sensitized solar cells, and decomposition of water pollution.

Acknowledgements

This work has been supported by the National Nanotechnology Center (NANOTEC) (P-10-1079), NSTDA, Ministry of Science and Technology, Thailand and through the NANOTEC program of the Centers of Excellence Network. Deep appreciation goes to Sakorn Minerals Co., Ltd., Thailand; to College of Nanotechnology, King Mongkut's Institute of Technology Ladkrabang (KMITL); and to Nanotechnology for Textile and Polymer Research Group (Nano-TeP) of Faculty of Engineering of Rajamangala University of Technology Thanyaburi (RMUTT) for a myriad of support and assistance.

References

[1] B. O'Regan, M. Grätzel, Nature 353 (1991) 737–740.
[2] N.G. Park, J. Lagemaat, A.J. Frank, J. Phys. Chem. B 104 (2000) 8989–8994.
[3] S.U.M. Khan, M. Al-Shahry, W.B. Ingler, Science 297 (2002) 2243–2245.
[4] J. Jitputti, S. Pavasupree, Y. Suzuki, S. Yoshikawa, J. Solid State Chem. 180 (2007) 1743–1749.
[5] J. Jitputti, Y. Suzuki, S. Yoshikawa, Catal. Commun. 9 (2008) 1265–1271.
[6] A. Fujishima, K. Honda, Nature 238 (1972) 37–38.
[7] H.J. Yun, H. Lee, J.B. Joo, W. Kim, J. Yi, J. Phys. Chem. C 113 (2009) 3050–3055.
[8] M.A. Fox, M.T. Dulay, Chem. Rev. 93 (1993) 341–357.
[9] X. Tao, W.H. Ma, T.Y. Zhang, J.Y. Zhao, Angew. Chem. Int. Ed. 40 (2001) 3014–3016.
[10] D.J. Yang, Z.F. Zheng, H.W. Liu, H.Y. Zhu, X.B. Ke, Y. Xu, D. Wu, Y. Sun, J. Phys. Chem. C 112 (2008) 16275–16280.
[11] J.Y. Li, C.C. Chen, J.C. Zhao, H.Y. Zhu, J. Orthman, Appl. Catal. B: Environ. 37 (2002) 331–338.
[12] K. Chen, J.Y. Li, J. Li, Y.M. Zhang, W.X. Wang, Colloids Surf. A: Physicochem. Eng. Aspects 360 (2010) 47–56.
[13] S.N. Frank, A.J. Bard, J. Am. Chem. Soc. 99 (1977) 303–305.
[14] K. Chen, J. Li, W. Wang, Y. Zhang, X. Wang, H. Su, Mater. Sci. Semicond. 15 (2012) 20–26.
[15] S. Sakulkhaemaruethai, S. Pavasupree, Y. Suzuki, S. Yoshikawa, Mater. Lett. 59 (2005) 2965–2968.
[16] F. Pan, J. Zhang, H. Liu, T. Wang, W. Hao, Key Eng. Mater. 280–283 (2005) 293–296.
[17] K. Koci, L. Obalova, L. Matejova, D. Placha, Z. Lacny, J. Jirkovsky, O. Solcova, Appl. Catal. B: Environ. 89 (2009) 494–502.
[18] A. Testino, I.R. Bellobono, V. Buscaglia, C. Canevali, M. D'Arienzo, S. Polizzi, R. Scotti, F. Morazzoni, J. Am. Chem. Soc. 129 (2007) 3564–3575.
[19] Ch. Boughelouma, A. Messalhi, Phys. Procedia 2 (2009) 1055–1058.
[20] J.-Y. Jung, C.-S. Lee, J. Ind. Eng. Chem. 17 (2011) 237–242.
[21] M. Grätzel, Nature 414 (2001) 338–344.
[22] I.C. Flores, J.N. de Freitas, C. Longo, M.-A. De Paoli, H. Winnischofer, A.F. Nogueira, J. Photochem. Photobiol. A: Chem. 189 (2007) 153–160.
[23] B.X. Wang, D.F. Xue, Y. Shi, F.H. Xue, in: W.V. Prescott, A.I. Schwartz (Eds.), Nanorods, Nanotubes and Nanomaterials Research Progress, New Nova Science Publishers Inc., New York, 2008.
[24] H. Hahn, R.S. Averback, Nanostruct. Mater. 1 (1992) 95–100.
[25] H. Yin, Y. Wada, T. Kitamura, S. Kambe, S. Murasawa, H. Mori, T. Sakata, S. Yanagida, J. Mater. Chem. 11 (2001) 1694–1703.
[26] M.K. Akhtar, S. Vermury, S.E. Pratsinis, Nanostruct. Mater. 4 (1994) 537–544.
[27] Z. Cai, J. Li, Y. Wang, J. Alloys Compd. 489 (2010) 167–169.
[28] Z. Zhang, C. Shao, L. Zhang, X. Li, Y. Liu, J. Colloid Interface Sci. 351 (2010) 57–62.
[29] S. Ngamsinlapasathian, T. Sreethawong, Y. Suzuki, S. Yoshikawa, Sol. Energy Mater. Sol. Cells 86 (2005) 269–282.
[30] T. Sreethawong, Y. Suzuki, S. Yoshikawa, J. Solid State Chem. 178 (2005) 329–338.
[31] T. Kasuga, M. Hiramatsu, A. Hoson, T. Sekino, K. Niihara, Langmuir 14 (1998) 3160–3163.
[32] T. Kasuga, M. Hiramatsu, A. Hoson, T. Sekino, K. Niihara, Adv. Mater. 11 (1999) 1307–1311.
[33] R. Yoshida, Y. Suzuki, S. Yoshikawa, Mater. Chem. Phys. 91 (2005) 409–416.
[34] Y. Suzuki, S. Pavasupree, S. Yoshikawa, R. Kawahata, J. Mater. Res. 20 (2005) 1063–1070.
[35] S. Pavasupree, Y. Suzuki, S. Yoshikawa, R. Kawahata, J. Solid State Chem. 178 (2005) 3110–3116.
[36] Y. Suzuki, S. Yoshikawa, J. Mater. Res. 19 (2004) 982–985.
[37] R. Yoshida, Y. Suzuki, S. Yoshikawa, J. Solid State Chem. 178 (2005) 2179–2185.
[38] S. Pavasupree, N. Laosiripojana, S. Chuangchote, T. Sagawa, Jpn. J. Appl. Phys. 50 (2011), 01BJ16-1–01BJ16-4.
[39] D. Aphairaj, T. Wirunmongkol, S. Pavasupree, P. Limsuwan, Energy Procedia 9 (2011) 539–544.
[40] A. Simpraditpan, T. Wironmongkol, S. Pavasupree, W. Pecharapa, Ceram. Int. 39 (2013) 2497–2502.
[41] Y.R. Smith, K.J.A. Raj, V. Subramanian, B. Viswanathan, Colloids Surf. A: Physicochem. Eng. Aspects 367 (2010) 140–147.
[42] T.K. Ghorai, M. Chakraborty, P. Pramanik, J. Alloys Compd. 509 (2011) 8158–8164.
[43] A. Nakahira, T. Kubo, C. Numako, Inorg. Chem. 49 (2010) 5845–5852.
[44] A.R. Armstrong, G. Armstrong, J. Canales, P.G. Bruce, Angew. Chem. Int. Ed. 43 (2004) 2286–2288.
[45] Z.-Y. Yuan, B.-Y. Su, Colloids Surf. A 241 (2004) 173–183.
[46] H.-L. Kuo, C.-Y. Kuo, C.-H. Liu, J.-H. Chao, C.-H. Lin, Catal. Lett. 113 (2007) 7–12.
[47] K.C. Song, S.E. Pratsinis, J. Colloid Interface Sci. 231 (2000) 289–298.
[48] C.L. Luu, Q.T. Nguyen, S.T. Ho, Adv. Nat. Sci.: Nanosci. Nanotechnol. 1 (2010) 015008.
[49] X.X. Slamet, H.W. Nasution, E. Purnama, S. Kosela, J. Gunlazuardi, Catal. Commun. 6 (2005) 313–319.
[50] Z.R.A. Spurr, H. Myers, Anal. Chem. 29 (2008) 760–763.
[51] G. Wang, L. Xu, J. Zhang, T. Yin, D. Han, Int. J. Photoenergy 2012 (2012) 265760.
[52] J.G. Yu, Y.R. Su, B. Cheng, Adv. Funct. Mater. 17 (2007) 1984–1990.
[53] S. Mozia, A. Heciak, A.W. Morawski, Appl. Catal. B: Environ. 104 (2011) 21–29.
[54] P. Górska, A. Zaleska, E. Kowalska, et al. Appl. Catal. B: Environ. 84 (2008) 440–447.
[55] C.C. Tsai, H. Teng, Chem. Mater. 16 (2004) 4352–4358.
[56] X. Deng, Y. Yue, Z. Gao, Appl. Catal. B 39 (2002) 135–147.
[57] B. Oregan, M. Grätzel, Nature 353 (1991) 737–739.
[58] Y. Liu, J.H. Wei, R. Xiong, C.X. Pan, J. Shi, Appl. Surf. Sci. 257 (2011) 8121–8126.
[59] M.A. Klan, S.I. Woo, O.B. Yang, Int. J. Hydrogen Energy 33 (2008) 5345–5351.
[60] Q. Xiao, L.L. Ouyang, Chem. Eng. J. 148 (2009) 248–253.
[61] L.L. Costa, A.G.S. Prado, J. Photochem. Photobiol. A: Chem. 201 (2009) 45–49.
[62] G.S. Guo, C.N. He, Z.N. Wang, F.B. Gu, D.M. Han, Talanta 72 (2007) 1687–1692.
[63] R.R. Bacsa, J. Kiwi, Appl. Catal. B 16 (1998) 19–29.
[64] T. Peng, D. Zhao, K. Dai, W. Shi, K. Hirao, J. Phys. Chem. B 109 (2005) 4947–4952.
[65] C.L. Wong, Y.N. Tan, A.R. Mohamed, J. Environ. Manage. 92 (2011) 1669–1680.
[66] J. Zhang, X. Xiao, J. Nan, J. Hazard. Mater. 176 (2010) 617–622.
[67] S. Kaewgun, D. Mckinney, J. White, A. Smith, M. Tinker, J. Ziska, B.I. Lee, J. Photochem. Photobiol. A: Chem. 202 (2009) 154–158.
[68] D. Gumy, C. Morais, P. Bowen, C. Pulgarin, S. Giraldo, R. Hajdu, J. Kiwi, Appl. Catal. B 63 (2006) 76–84.
[69] S. Pavasupree, J. Jitputti, S. Ngamsinlapasathian, S. Yoshikawa, Mater. Res. Bull. 43 (2008) 149–157.
[70] Z. Zhu, X. Li, Q. Zhao, Z. Qu, Y. Hou, L. Zhao, S. Liu, G. Chen, Mater. Res. Bull. 45 (2010) 1889–1893.
[71] R. Mu, Z. Xu, L. Li, Y. Shao, H. Wan, S. Zheng, J. Hazard. Mater. 176 (2010) 495–502.
[72] H.H. Ou, C.H. Liao, Y.H. Liou, J.H. Hong, S.L. Lo, Environ. Sci. Technol. 42 (2008) 4507–4512.
[73] S. Song, J.J. Tu, Z.Q. He, F.Y. Hong, W.P. Liu, J.M. Chen, Appl. Catal. A 378 (2010) 169–174.
[74] A. Yamakata, T. Ishibashi, H. Onishi, J. Mol. Catal. A: Chem. 199 (2003) 85–94.

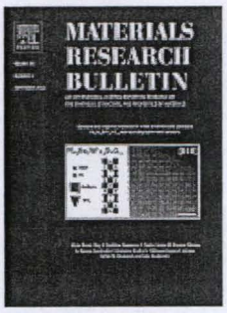

Materials Research Bulletin

An international journal reporting research on the synthesis, structure, and properties of materials

Materials Research Bulletin is an international rapid publication journal reporting research on the synthesis, processing, structure and properties of **inorganic materials** with interesting **electronic**, **magnetic**...

View full aims and scope

Editor-in-Chief: Professor M. Greenblatt
View full editorial board

Guide for Authors
Submit Your Paper
Track Your Paper
Order Journal
View Articles

Impact Factor: 1.913

5-Year Impact Factor: 2.141

Imprint: ELSEVIER

ISSN: 0025-5408

Stay up-to-date

Register your interests and receive email alerts tailored to your needs

Click here to sign up

Follow us

Subscribe to RSS

Latest News

Most Downloaded Articles

1. Issue and challenges facing rechargeable thin film lithium batteries
Arun Patil | Vaishali Patil | ...

2. Aqueous chemical growth of Cu2ZnSnS4 (CZTS) thin films: Air annealing and photoelectrochemical properties
N.M. Shinde | P.R. Deshmukh | ...

3. Silver nanowire based flexible electrodes with improved properties: High conductivity, transparency, adhesion and low haze
A.B.V. Kiran Kumar | Chang wan Bae | ...

VIEW ALL

Materials Science News

Fundamental size-dependence for nanocrystals undergoing phase transitions
30 August 2013

Building nanotubes with specific, predictable atomic structures
29 August 2013

Novel polymer helps medication reach the bloodstream
29 August 2013

Liquid calcium carbonate?
28 August 2013

VIEW ALL

Journal Insights

Discover this journal's metrics

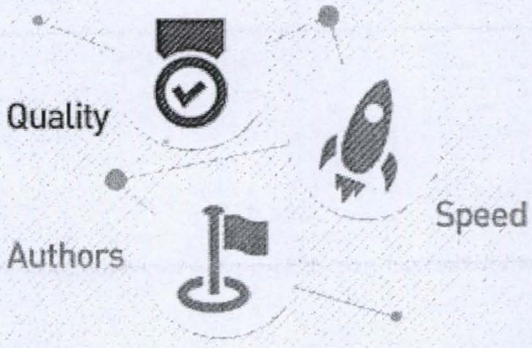

FIND OUT MORE

News

All Elsevier Materials Science journals now offer a new, free service to authors: AudioSlides
These are brief, webcast-style presentations based on slides and audio that are shown next to the article on ScienceDirect.

Announcing 3 new editors

Robert Cahn Award Winner Announced

VIEW ALL

Podcasts

AFM-based infrared spectroscopy
30 August 2013

Bioelectronics Part 2
21 August 2013